Supporting Information

Three-Dimensional Topotactic Host Structure Secured Ultra-Stable VP-CNOs Composite Anode for Long Lifespan Lithium and Sodium Ion Capacitors

Wenbo Cheng,[†,‡,§] Biao Wan,[†] Shishuai Xu,[¶] Miaoxin Zhang, [‡,§] Rongguang Zeng,[⊥] Zexin Liu[a], [‡,§] Chengwei Zhang, [‡,§] Fuxing Yin, [‡,§] Gongkai Wang, [‡,§]* Huiyang Gou[†]*

[†] Center for High Pressure Science and Technology Advanced Research, Beijing 100094, China

[‡] School of Material Science and Engineering, Research Institute for Energy Equipment Materials, Hebei University of Technology, Tianjin, 300130, China

[§] Tianjin Key Laboratory of Materials Laminating Fabrication and Interface Control Technology, Hebei University of Technology, Tianjin 300130, China

[¶] State Key Laboratory of Metastable Materials Science and Technology， Yanshan University, Qinhuangdao, 066004, China

[⊥] Institute of Materials, China Academy of Engineering Physics, P.O. Box 9071, Jiangyou, Sichuan 621907, China

Corresponding authors

*E-mail addresses: wang.gongkai@hebut.edu.cn (G. K. Wang)

*E-mail addresses: huiyang.gou@hpstar.ac.cn (H. Y. Gou)

Table S1. Lattice parameters and atomic position of Li/NaVP and Li_2/Na_2VP

Compound	Lattice parameters		Atom	Site	Special Position		
	a	c			x	y	z
LiVP	4.047	5.007	V	2a	0	0	0
			P	2c	0.3333	0.6667	0.25
			Li	2d	0.6667	0.3333	0.25
NaVP	4.463	5.283	V	2a	0	0	0
			P	2c	0.3333	0.6667	0.25
			Na	2d	0.6667	0.3333	0.25
Li_2VP	4.144	6.372	V	2a	0	0	0
			P	2c	0.3333	0.6667	0.25
			Na	4f	0.6667	0.3333	0.0999
Na_2VP	4.778	7.625	V	2a	0	0	0
			P	2c	0.3333	0.6667	0.25
			Na	4f	0.6667	0.3333	0.0987

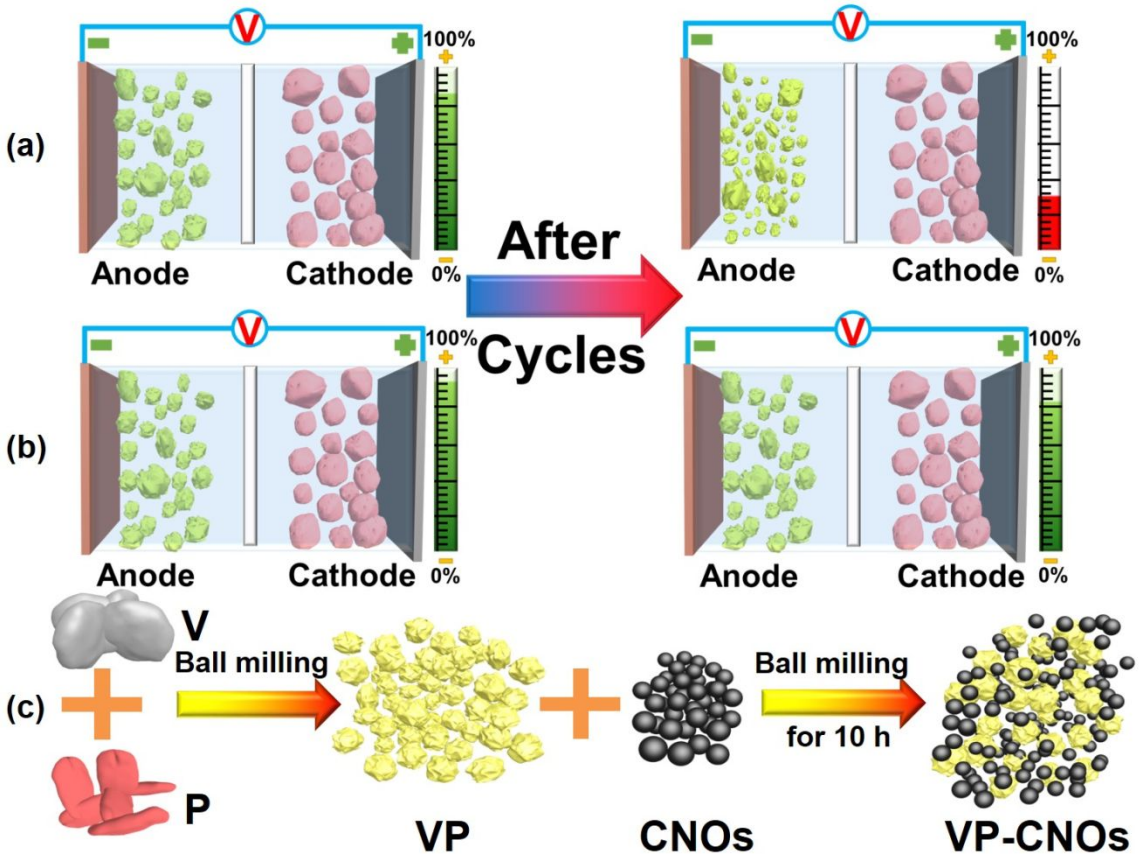

Figure S1. (a) and (b) Schematic illustration of LICs/SICs degradation based on different types of anode. (c) Schematic illustration of synthesis process of VP and VP-CNOs by high energy ball milling.

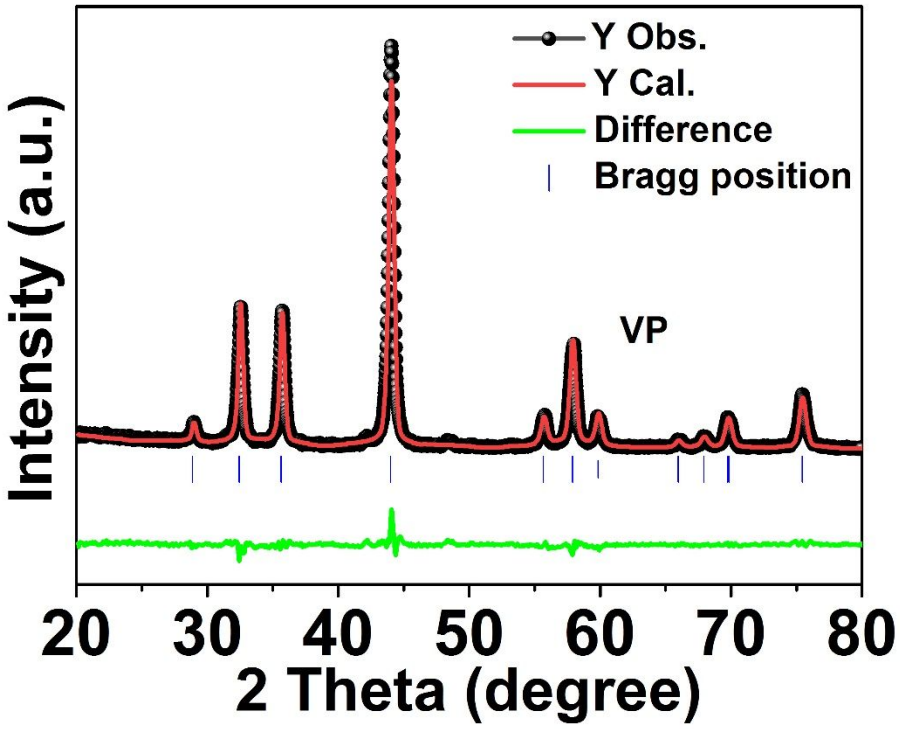

Figure S2. Rietveld refined XRD pattern of VP.

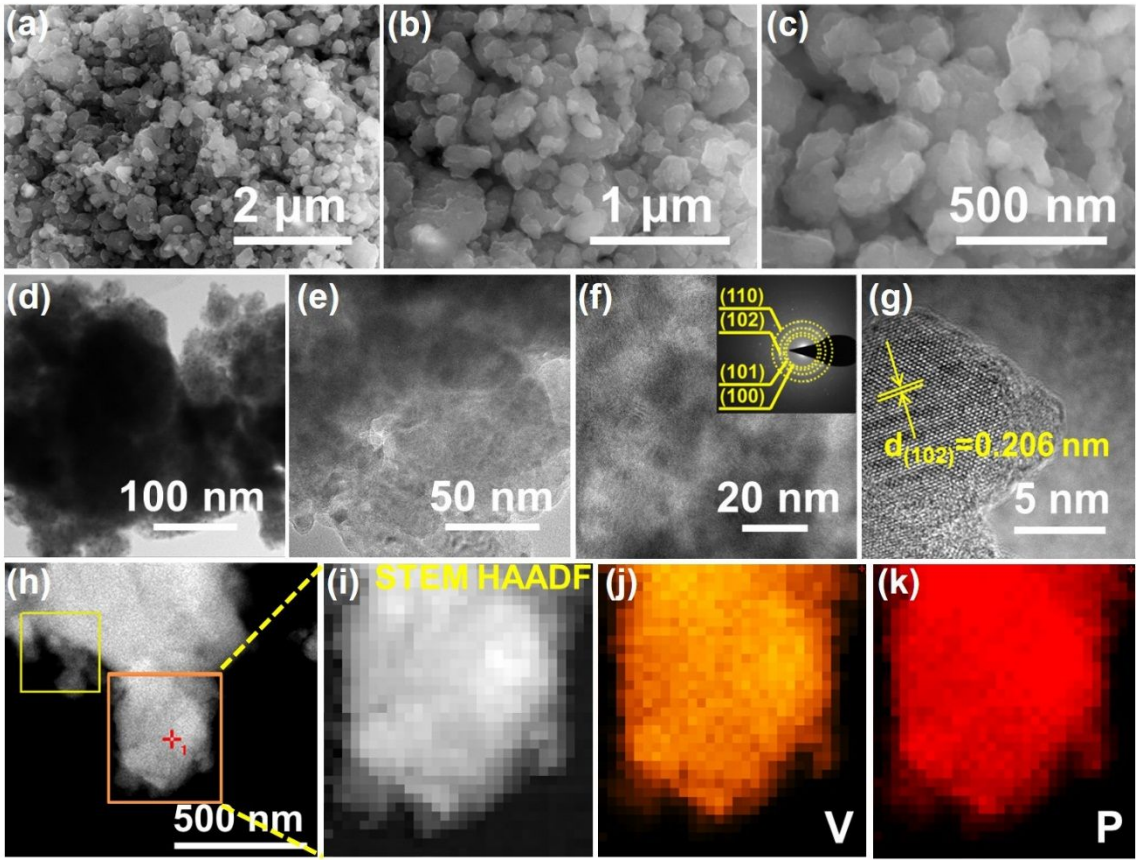

Figure S3. Morphology characterization of VP. (a-c) SEM images. (d-g) TEM images. (h-k) EDS mapping.

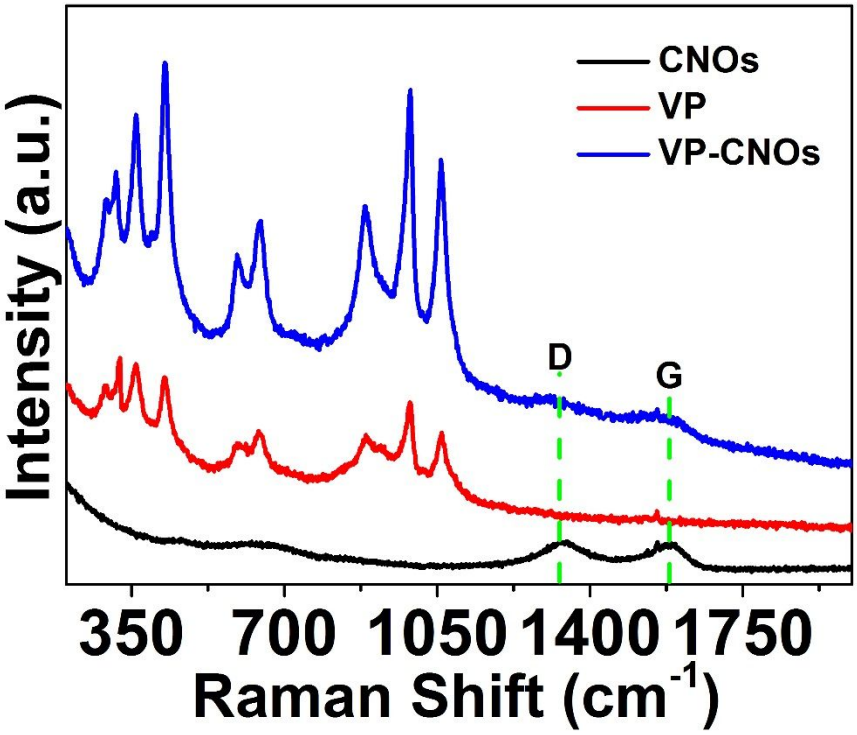

Figure S4. Raman spectra of VP, VP-CNOs, and CNOs. D and G bands correspond to CNOs, indicating the disordered and graphitic carbon. Characteristic peaks in range from 100 to 1200 cm^{-1} are indexed into vibration models of VP.

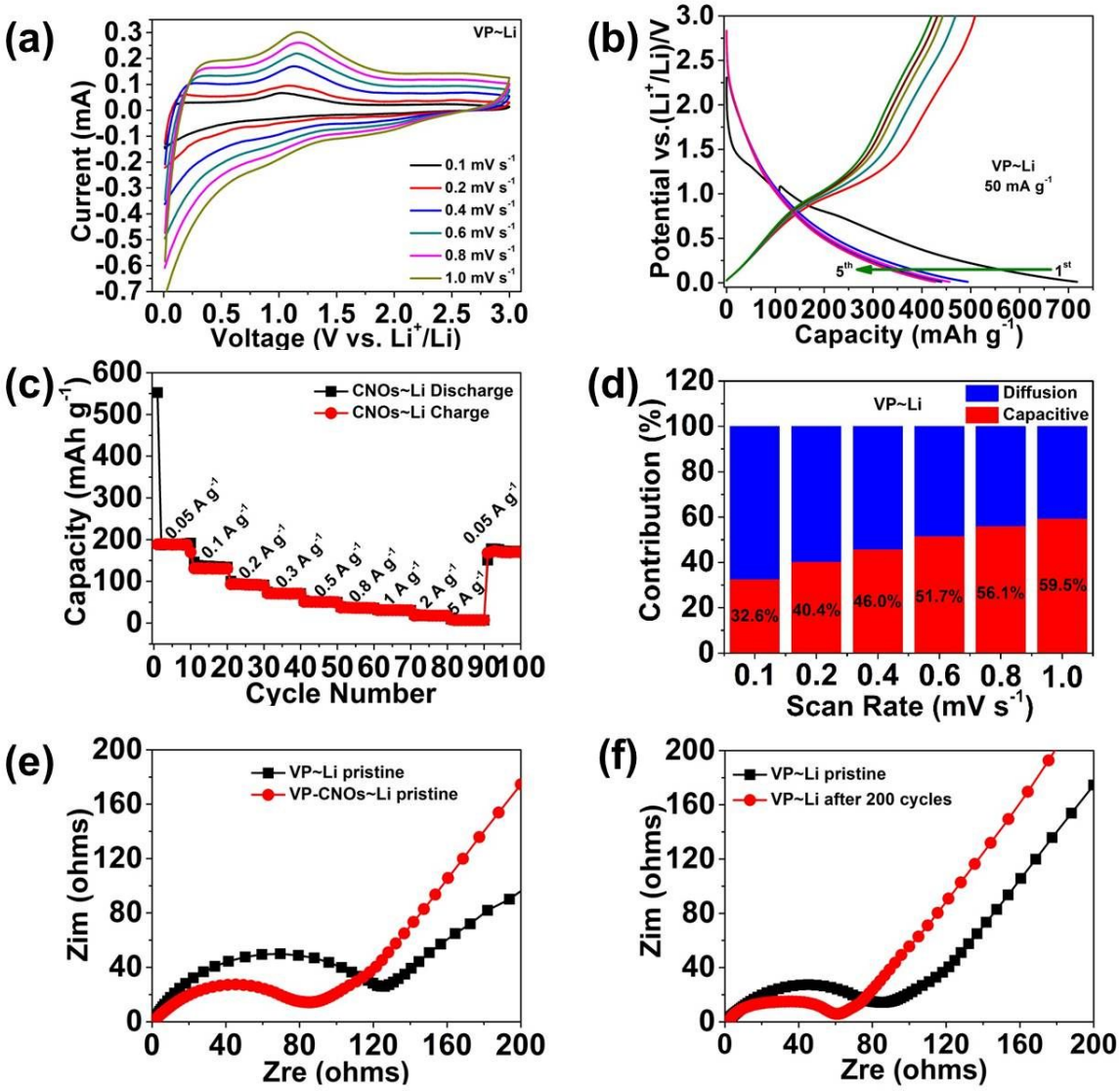

Figure S5. Electrochemical performance vs. Li^+. (a) and (b) CV curves and charge/discharge potential profiles of VP. (c) Rate performance of CNOs. (d) Contribution ratio at various scan rates of VP. (e, f) EIS spectra of pristine and 200 cycled VP and VP-CNOs.

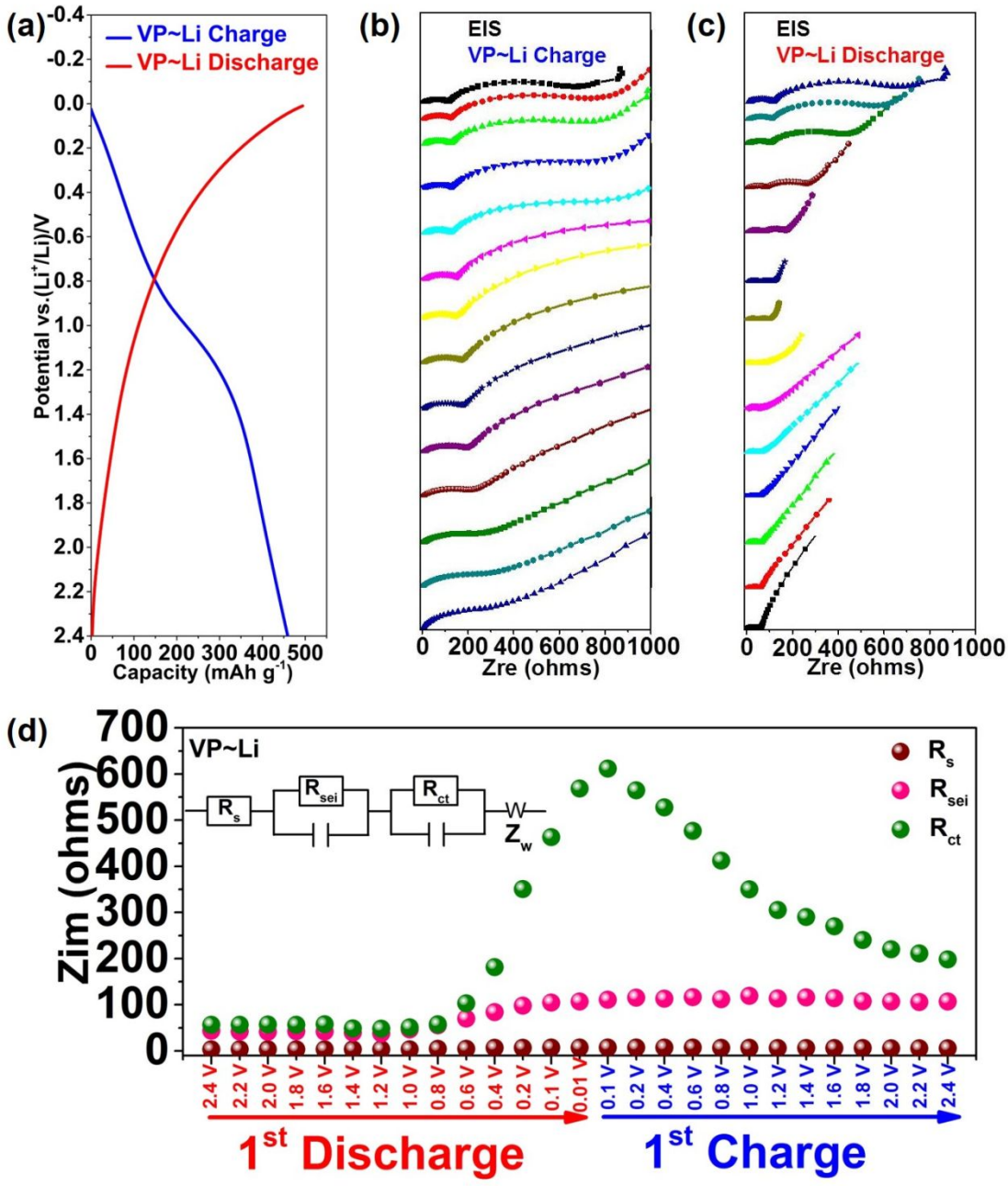

Figure S6. *In-situ* EIS spectra of VP vs. Li^+. (a) Initial charge/discharge curve. (b) and (c) EIS spectra of charge and discharge process, respectively. (d) Fitted results of R_s, R_{sei}, and R_{ct} of VP, and corresponding equivalent electrical circuit (inset).

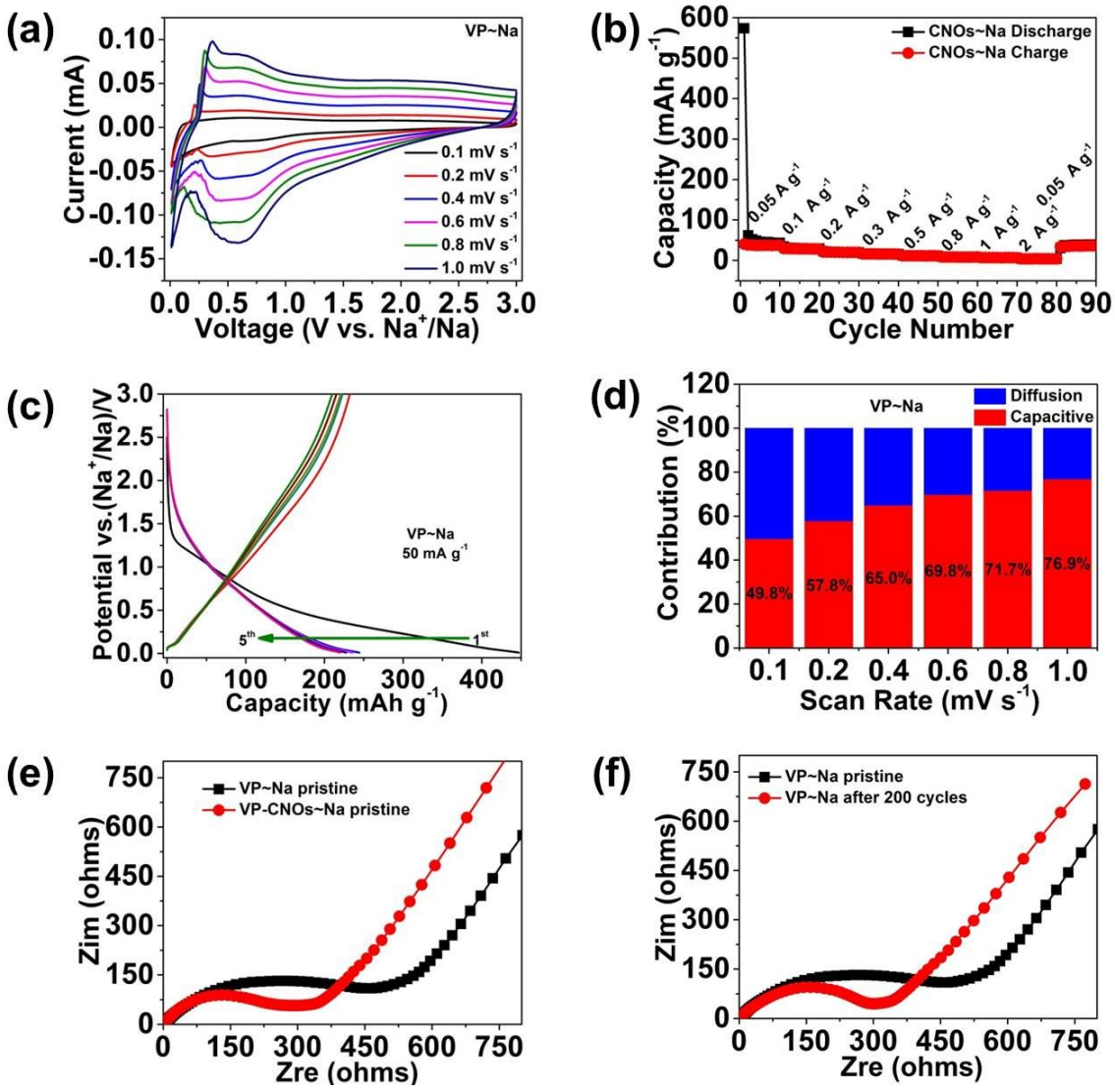

Figure S7. Electrochemical performance vs. Na^+. (a) and (c) CV curves and charge/discharge potential profiles of VP. (b) Rate performance of CNOs. (d) Contribution ratio at various scan rates of VP. (e, f) EIS spectra of pristine and 200 cycled VP and VP-CNOs.

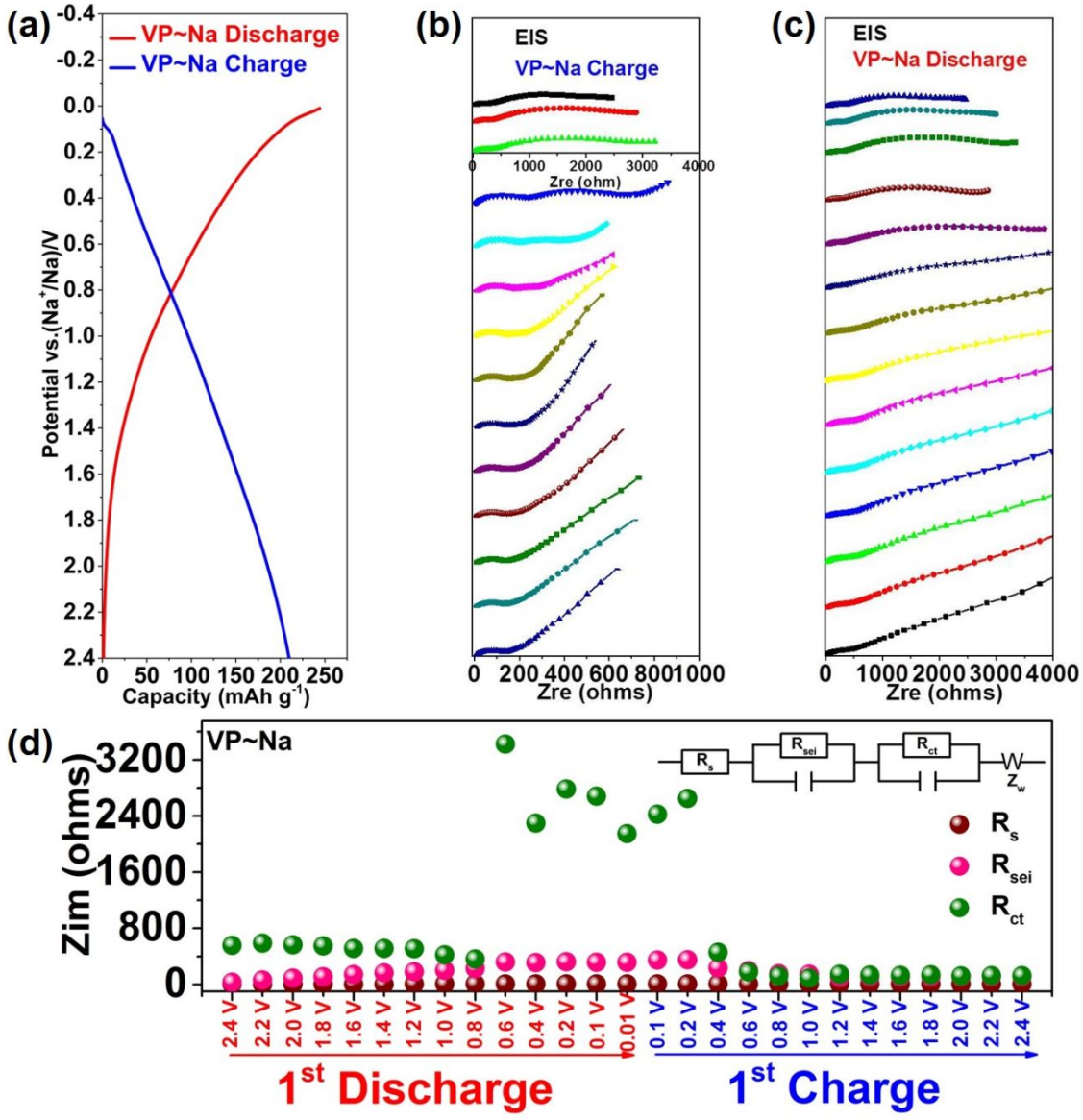

Figure S8. *In-situ* EIS spectra of VP vs. Na^+. (a) Initial charge/discharge curve. (b) and (c) EIS spectra of charge and discharge process, respectively. (d) Fitted results of R_s, R_{sei}, and R_{ct} of VP, and corresponding equivalent electrical circuit (inset).

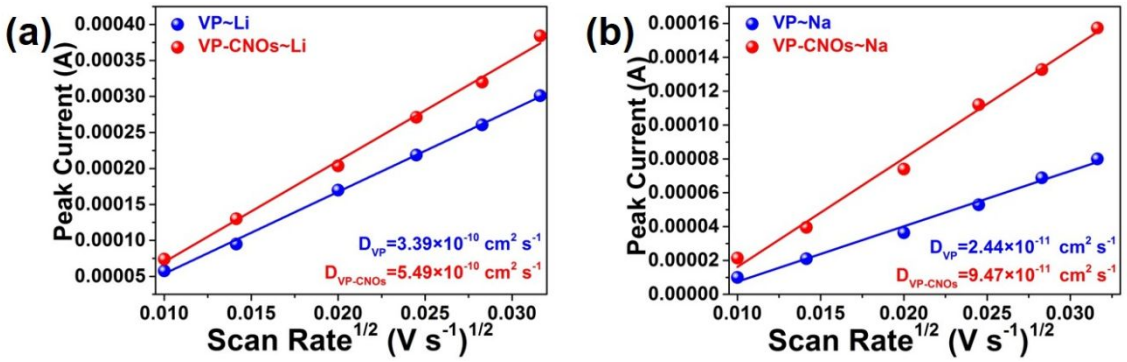

Figure S9. Dependence of peak current on the square root of the scan rate of VP/VP-CNOs vs. Li/Na.

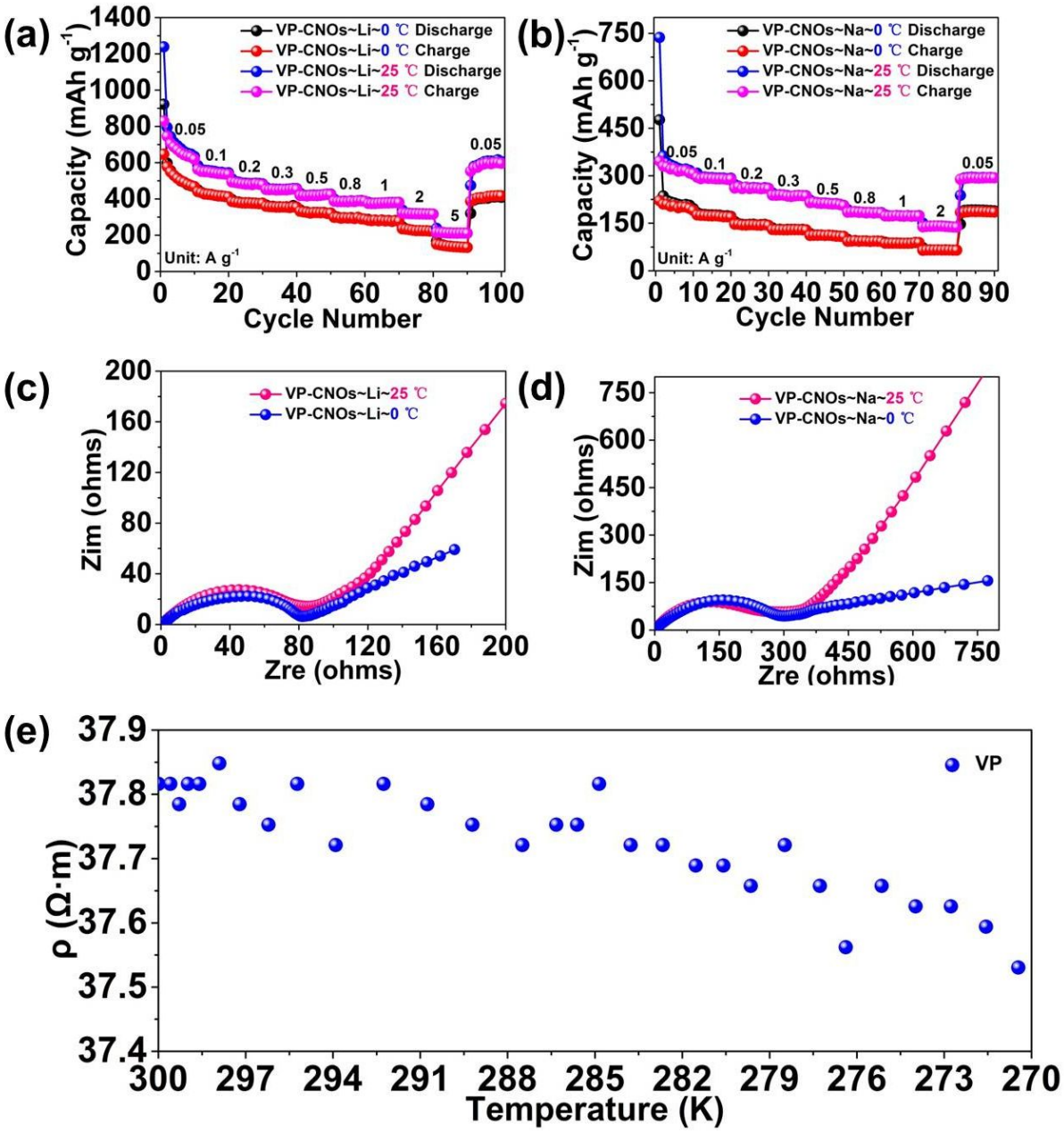

Figure S10. Electrochemical performance of VP-CNOs at low temperature (0 °C). (a) Rate performance vs. Li. (b) Rate performance vs. Na. (c) EIS spectra vs. Li. (d) EIS spectra vs. Na. (e) Electronic resistance variation as a functional of temperature. The decrease of rate performance are observed apparently (average decrease of 22% vs. Li, 48% vs. Na), however, this decrease is mainly attributed to the severe increase of diffusion impedance of electrolyte (Nyquist plot), rather than VP-CNOs itself, whereas the electronic resistance

of VP is decreased as the decrease of temperature, demonstrating the promising physical feature of VP.

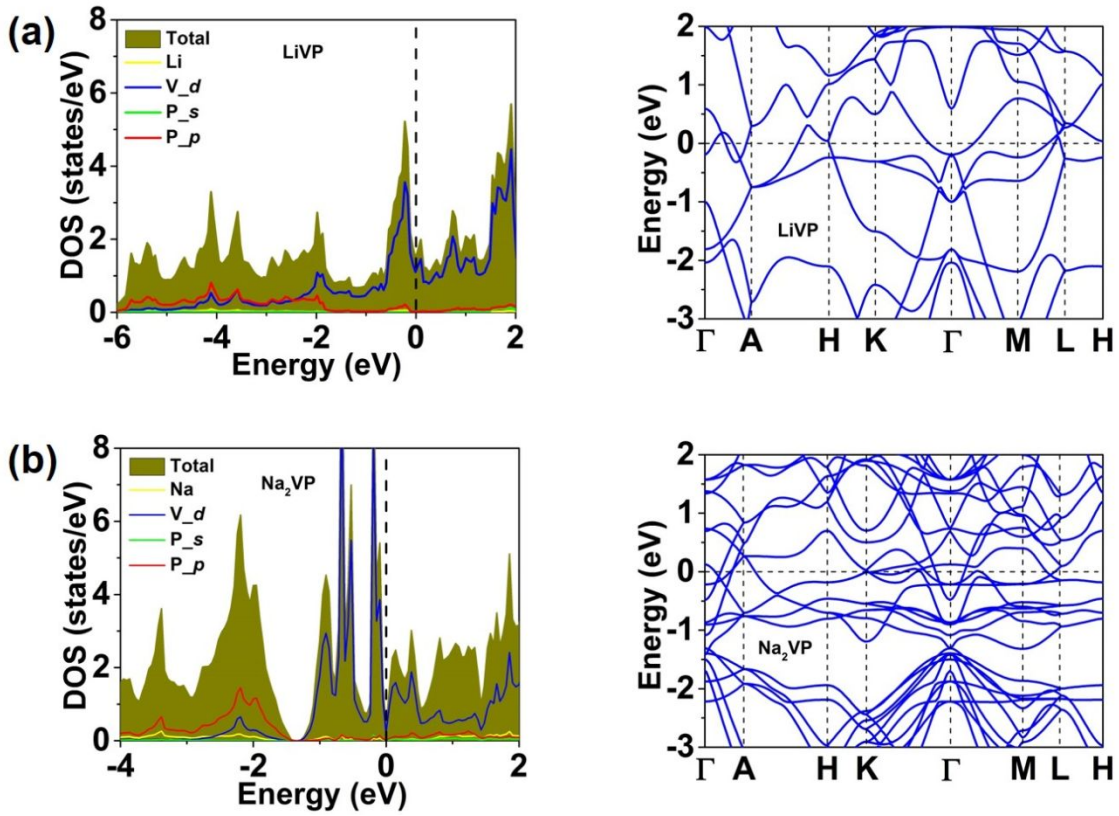

Figure S11. The calculated band structure and total/partial DOSs of LiVP and Na_2VP.

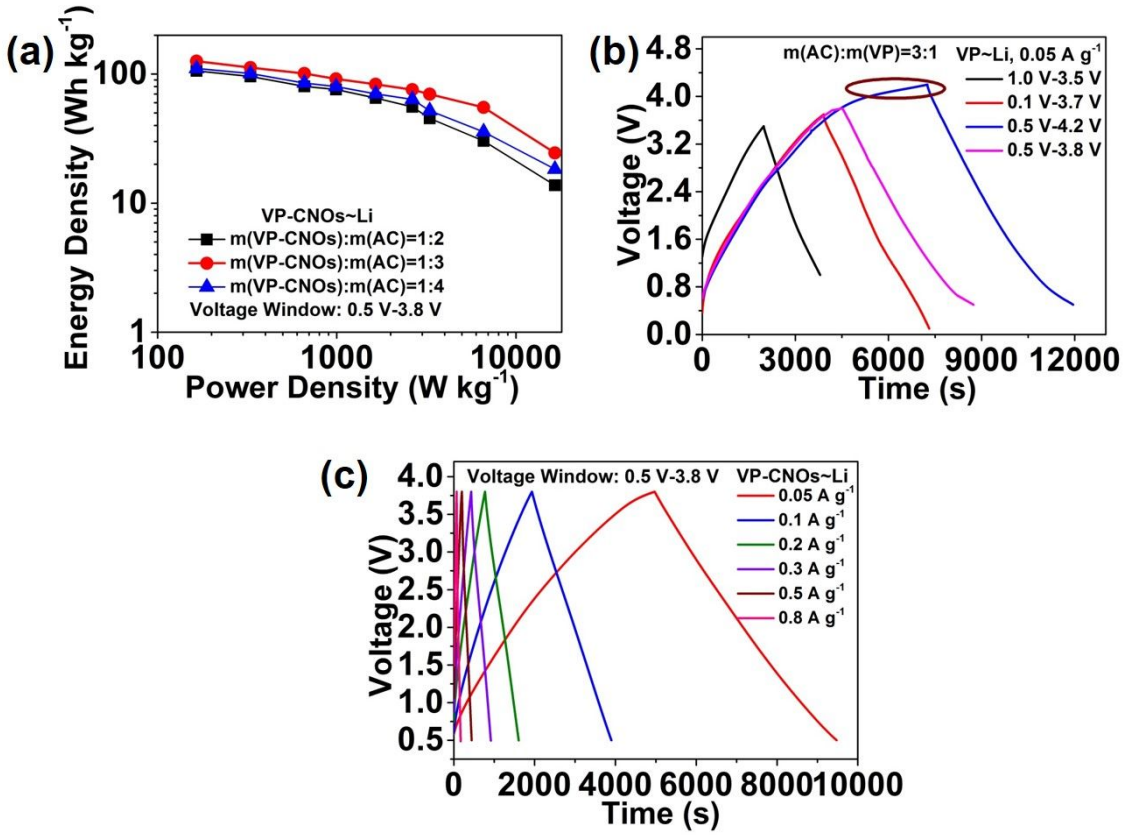

Figure S12. Optimization of LICs. (a) Ragone plots of LICs based on VP-CNOs anode and AC cathode under various mass ratios. (b) Various voltage windows of LICs based on the mass ratio of 1:3 (anode: cathode) at 0.05 A g^{-1}. (c) Galvanostatic charge/discharge profiles of LICs with the mass ratio of 1:3 under the voltage window of 0.5-3.8V.

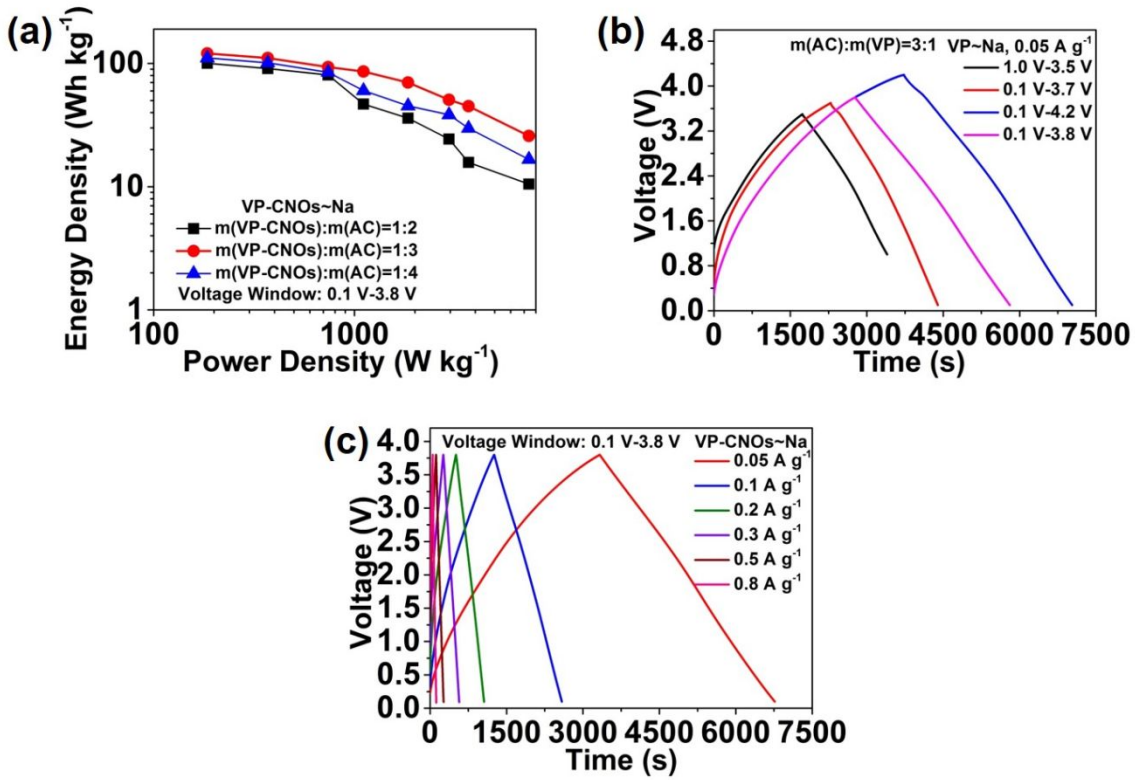

Figure S13. Optimization of SICs. a) Ragone plots of SICs based on VP-CNOs anode and AC cathode under various mass ratios. b) Various voltage windows of SICs based on the mass ratio of 1:3 (anode: cathode) at 0.05 A g^{-1}. c) Galvanostatic charge/discharge profiles of SICs with the mass ratio of 1:3 under the voltage window of 0.1-3.8V.

Figure S14. Photograph of the preservative film covered on the electrode.

Reference (Lithium/sodium ion diffusion coefficient comparison)

(1) Liu, Z.; Zhang, X.; Huang, D.; Gao, B.; Ni, C.; Wang, L.; Ren, Y.; et al. Confined seeds derived sodium titanate/graphene composite with synergistic storage ability toward high performance sodium ion capacitors. *Chem. Eng. J.* **2020**, *379*, 122418.
(2) Wang, Y.; Zhang, X.; Xiong, P.; Yin, F.; Xu, Y.; Wan, B.; Wang, Q.; et al. Insight into the intercalation mechanism of WSe2 onions toward metal ion capacitors: sodium rivals lithium. *J. Mater. Chem. A* **2018**, *6*, 21605-21617.
(3) Jin, L.; Gong, R.; Zhang, W.; Xiang, Y.; Zheng, J.; Xiang, Z.; Zhang, C.; et al. Toward high energy-density and long cycling-lifespan lithium ion capacitors: a 3D carbon modified low-potential Li2TiSiO5 anode coupled with a lignin-derived activated carbon cathode. *J. Mater. Chem. A* **2019**, *7*, 8234-8244.
(4) Yu, P.; Popov, B. N.; Ritter, J. A.; White, R. E. Determination of the Lithium Ion Diffusion Coefficient in Graphite. *J. Electrochem. Soc.* **1999**, *146*, 8-14.
(29) Guo, H.-j.; Li, X.-h.; Zhang, X.-m.; Wang, H.-q.; Wang, Z.-x.; Peng, W.-j. Diffusion coefficient of lithium in artificial graphite, mesocarbon microbeads, and disordered carbon. *New Carbon Mater.* **2007**, *22*, 7-10.
(5) Xu, G. B.; Li, W.; Yang, L. W.; Wei, X. L.; Ding, J. W.; Zhong, J. X.; Chu, P. K. Highly-crystalline ultrathin $Li_4Ti_5O_{12}$ nanosheets decorated with silver nanocrystals as a high-performance anode material for lithium ion batteries. *J. Power Sources* **2015**, *276*, 247-254.
(6) Zhang, C.; Song, H.; Liu, C.; Liu, Y.; Zhang, C.; Nan, X.; Cao, G. Fast and Reversible Li Ion Insertion in Carbon-Encapsulated Li_3VO_4 as Anode for Lithium-Ion Battery. *Adv. Funct. Mater.* **2015**, *25*, 3497-3504.
(7) Liu, Q.; Li, Z.-F.; Liu, Y.; Zhang, H.; Ren, Y.; Sun, C.-J.; Lu, W.; et al. Graphene-modified nanostructured vanadium pentoxide hybrids with extraordinary electrochemical performance for Li-ion batteries. *Nat. Commun.* **2015**, *6*, 6127.
(8) Deng, B.; Lei, T.; Zhu, W.; Xiao, L.; Liu, J. In-Plane Assembled Orthorhombic Nb_2O_5 Nanorod Films with High-Rate Li+ Intercalation for High-Performance Flexible Li-Ion Capacitors. *Adv. Funct. Mater.* **2018**, *28*, 1704330.
(9) Wang, J.; Polleux, J.; Lim, J.; Dunn, B. Pseudocapacitive Contributions to Electrochemical Energy Storage in TiO_2 (Anatase) Nanoparticles. *J. Phys. Chem. C* **2007**, *111*, 14925-14931.
(10) Liu, X.; Li, W.; Zhao, X.; Liu, Y.; Nan, C.-W.; Fan, L.-Z. Two Birds with One Stone: Metal–Organic Framework Derived Micro-/Nanostructured Ni_2P/Ni Hybrids Embedded in Porous Carbon for Electrocatalysis and Energy Storage. *Adv. Funct. Mater.* **2019**, *29*, 1901510.
(11) Li, Q.; Li, L.; Wu, P.; Xu, N.; Wang, L.; Li, M.; Dai, A.; et al. Silica Restricting the Sulfur Volatilization of Nickel Sulfide for High-Performance Lithium-Ion Batteries. *Adv. Energy Mater.* **2019**, *9*, 1901153.
(12) Ge, P.; Hou, H.; Banks, C. E.; Foster, C. W.; Li, S.; Zhang, Y.; He, J.; et al. Binding $MoSe_2$ with carbon constrained in carbonous nanosphere towards high-capacity and ultrafast Li/Na-ion storage. *Energy Storage Mater.* **2018**, *12*, 310-323.
(13) Liu, C.; Zhang, C.; Song, H.; Zhang, C.; Liu, Y.; Nan, X.; Cao, G. Mesocrystal MnO cubes as anode for Li-ion capacitors. *Nano Energy* **2016**, *22*, 290-300.

(14) Yan, Y.; Ben, L.; Zhan, Y.; Huang, X. Nano-Sn embedded in expanded graphite as anode for lithium ion batteries with improved low temperature electrochemical performance. *Electrochim. Acta* **2016**, *187*, 186-192.
(15) Lee, Y.-W.; Kim, D.-M.; Kim, S.-J.; Kim, M.-C.; Choe, H.-S.; Lee, K.-H.; Sohn, J. I.; et al. In Situ Synthesis and Characterization of Ge Embedded Electrospun Carbon Nanostructures as High Performance Anode Material for Lithium-Ion Batteries. *ACS Appl. Mat. Interfaces* **2016**, *8*, 7022-7029.
(16) Xin, F.-X.; Tian, H.-J.; Wang, X.-L.; Xu, W.; Zheng, W.-G.; Han, W.-Q. Enhanced Electrochemical Performance of $Fe_{0.74}Sn_5$@Reduced Graphene Oxide Nanocomposite Anodes for Both Li-Ion and Na-Ion Batteries. *ACS Appl. Mat. Interfaces* **2015**, *7*, 7912-7919.
(17) Guo, Q.; Ru, Q.; Liu, Y.; Yan, H.; Wang, B.; Hou, X. One-Step Fabrication of Carbon Nanotubes-Decorated Sn4P3 as a 3D Porous Intertwined Scaffold for Lithium-Ion Batteries. *ChemElectroChem* **2018**, *5*, 2150-2156.
(18) Kondo, Y.; Fukutsuka, T.; Miyazaki, K.; Miyahara, Y.; Abe, T. Investigation of Electrochemical Sodium-Ion Intercalation Behavior into Graphite-Based Electrodes. *J. Electrochem. Soc.* **2019**, *166*, A5323-A5327.
(19) Xiao, L.; Cao, Y.; Henderson, W. A.; Sushko, M. L.; Shao, Y.; Xiao, J.; Wang, W.; et al. Hard carbon nanoparticles as high-capacity, high-stability anodic materials for Na-ion batteries. *Nano Energy* **2016**, *19*, 279-288.
(20) Cao, B.; Liu, H.; Xu, B.; Lei, Y.; Chen, X.; Song, H. Mesoporous soft carbon as an anode material for sodium ion batteries with superior rate and cycling performance. *J. Mater. Chem. A* **2016**, *4*, 6472-6478.
(21) Li, M.; Xiao, X.; Fan, X.; Huang, X.; Liu, Y.; Chen, L. Carbon coated sodium-titanate nanotube as an advanced intercalation anode material for sodium-ion batteries. *J. Alloys Compd.* **2017**, *712*, 365-372.
(22) Chen, J.; Zhou, X.; Mei, C.; Xu, J.; Wong, C.-P. Improving the sodiation performance of Na2Ti3O7 through Nb-doping. *Electrochim. Acta* **2017**, *224*, 446-451.
(23) Wang, L.; Bi, X.; Yang, S. Partially Single-Crystalline Mesoporous Nb_2O_5 Nanosheets in between Graphene for Ultrafast Sodium Storage. *Adv. Mater.* **2016**, *28*, 7672-7679.
(24) Ghosh, S.; Kiran Kumar, V.; Kumar, S. K.; Biswas, S.; Martha, S. K. An insight of sodium-ion storage, diffusivity into TiO_2 nanoparticles and practical realization to sodium-ion full cell. *Electrochim. Acta* **2019**, *316*, 69-78.
(25) Pan, Y.; Cheng, X.; Gong, L.; Shi, L.; Zhang, H. Nanoflower-like N-doped C/CoS_2 as high-performance anode materials for Na-ion batteries. *Nanoscale* **2018**, *10*, 20813-20820.
(26) Zhao, X.; Cai, W.; Yang, Y.; Song, X.; Neale, Z.; Wang, H.-E.; Sui, J.; et al. $MoSe_2$ nanosheets perpendicularly grown on graphene with Mo–C bonding for sodium-ion capacitors. *Nano Energy* **2018**, *47*, 224-234.
(27) Ren, W.; Zhang, H.; Guan, C.; Cheng, C. Ultrathin MoS_2 Nanosheets@Metal Organic Framework-Derived N-Doped Carbon Nanowall Arrays as Sodium Ion Battery Anode with Superior Cycling Life and Rate Capability. *Adv. Funct. Mater.* **2017**, *27*, 1702116.
(28) Mi, H.; Wang, Y.; Chen, H.; Sun, L.; Ren, X.; Li, Y.; Zhang, P. Boosting Na-ion diffusion by piezoelectric effect induced by alloying reaction of micro red-phosphorus/$BaTiO_3$/graphene composite anode. *Nano Energy* **2019**, *66*, 104136.

(29) Meng, W.; Guo, M.; Liu, X.; Chen, J.; Bai, Z.; Wang, Z. Spherical nano Sb@HCMs as high-rate and superior cycle performance anode material for sodium-ion batteries. *J. Alloys Compd.* **2019**, *795*, 141-150.
(30) Lu, X.; Luo, F.; Xiong, Q.; Chi, H.; Qin, H.; Ji, Z.; Tong, L.; et al. Sn-MOF derived bimodal-distributed SnO_2 nanosphere as a high performance anode of sodium ion batteries with high gravimetric and volumetric capacities. *Mater. Res. Bull.* **2018**, *99*, 45-51.
(31) Cui, J.; Yao, S.; Huang, J.-Q.; Qin, L.; Chong, W. G.; Sadighi, Z.; Huang, J.; et al. Sb-doped SnO_2/graphene-CNT aerogels for high performance Li-ion and Na-ion battery anodes. *Energy Storage Mater.* **2017**, *9*, 85-95.